nanomaterials

MDPI

Supplementary Materials

Impact of Thermally Reducing Temperature on Graphene Oxide Thin Films and Microsupercapacitor Performance

Vusani M. Maphiri, Daba T. Bakhoum, Samba Sarr, Ndeye F. Sylla, Gift Rutavi and Ncholu Manyala *

Department of Physics, Institute of Applied Materials, SARChI Chair in Carbon Technology and Materials, University of Pretoria, Pretoria 0028, South Africa; vusanimuswamaphiri@gmail.com (V.M.M.); thiogna@yahoo.fr (D.T.B.); ssarr3112@gmail.com (S.S.); ntoufasylla@gmail.com (N.F.S.); rutavigift@yahoo.com (G.R.)

* Correspondence: ncholu.manyala@up.ac.za; Tel.: +27-12-420-3549; Fax: +27-12-420-3546

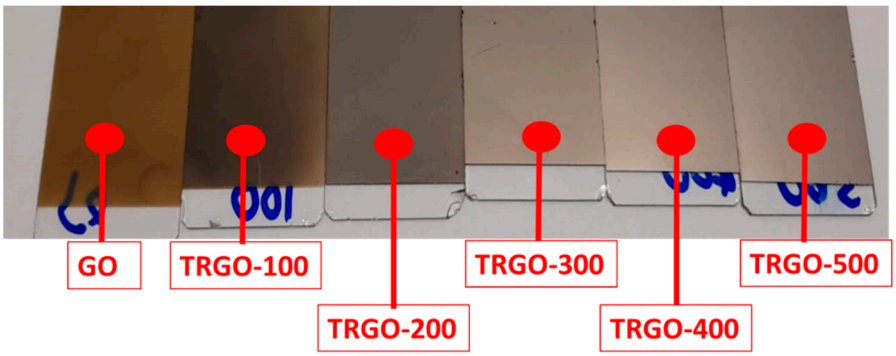

Figure S1. The digital images showing the appearance (colour) of the prepared thin film on MSG.

Figure S2a shows the interspacing distance of Graphite, GO and TRGO thin films. The interspacing distance of the TRGO-100 to TRGO-300 could not be calculated because of the diffraction peak of the MSG which has occurred at the same passion as the TRGO. This can be seen on Figure 2 and Figure S1b–d.

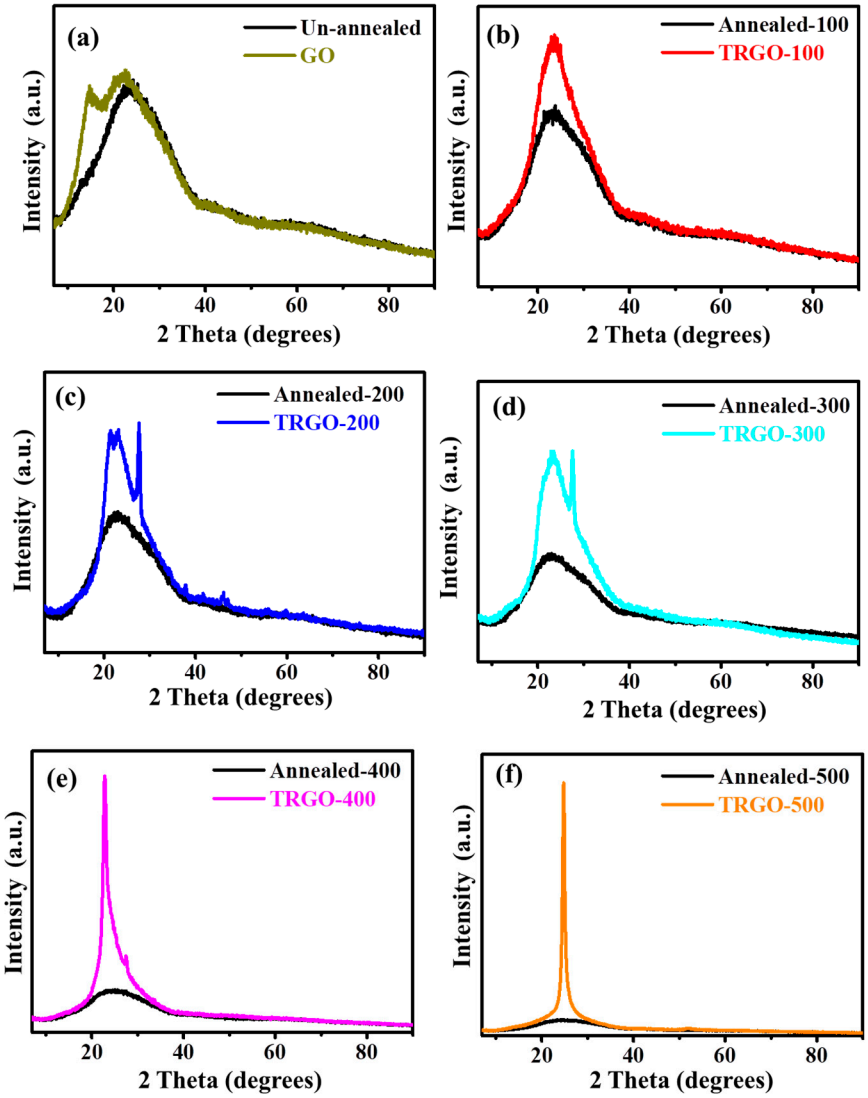

Figure S2. The XRD patterns of (a) GO and **(b)–(f)** TRGO-100 to TRGO-500, plotted together with the diffraction pattern of the microscopic glass under the same conditions.

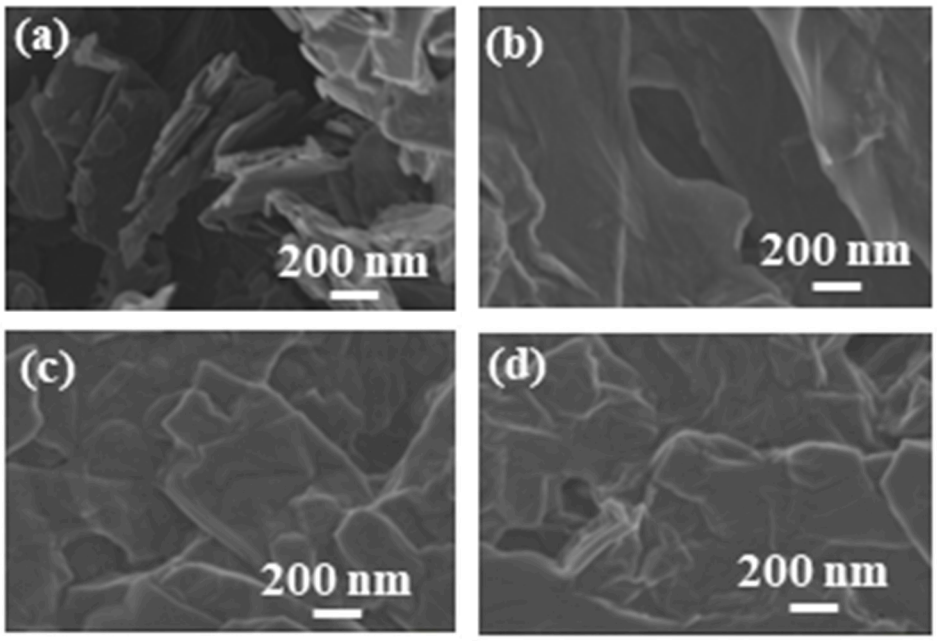

Figure S3. SEM images of (a) graphite, (b) GO, (c) TRGO-300 and (d) TRGO-500.

Surface Topography

The three-dimensional AFM images of the GO and TRGO samples are displayed in Figure S4 (a)–(f), while the corresponding colour scale is displayed in Fig.ureS4 (g) and the Roughness parameter are displayed on Table S1. The AFM of GO and TRGO-100 shows an average sheet height of approximately 1–1.5 μm due to the presence of the surface oxygen functional group. After the thermal reduction process, it can be easily elucidated that average sheet height has dramatically reduced due to the reduced oxygen content encouraging the van der Waals force through the π–π interaction of the adjacent sheet from restacking. The spike-like feathers at TRGO-200 to TRGO-500 are due to the wrinkle and crumbling of the GO sheets during the TR process.

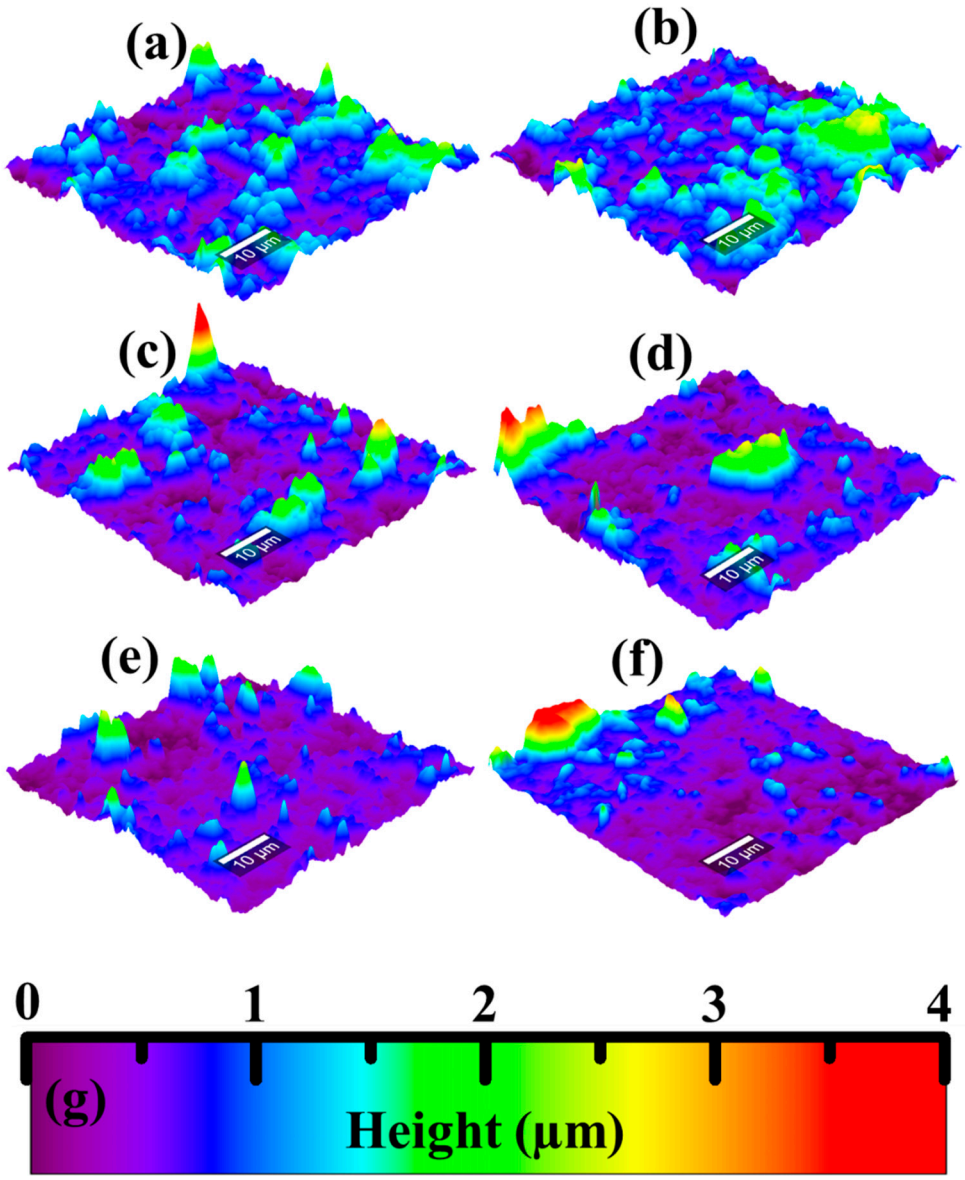

Figure S4. The AFM micrograph of **(a)** GO and **(b)–(f)** TRGO-100 to TRGO-500; and **(g)** corresponding height colour scale.

Table S1. Roughness parameter of the prepared GO/TRGO thin film.

Roughness Parameters	GO	TRGO-100	TRGO-200	TRGO-300	TRGO-400	TRGO-500
Number of Pixels	262144	262144	262144	262144	262144	262144
True Area [µm²]	3893.59	3939.16	3886.2	3827.2	3792.93	3803.26
Reference Area [µm²]	3585.95	3585.95	3585.95	3585.95	3585.95	3585.95
SDR [%]	9.11892	10.5894	9.02563	7.27021	6.28532	6.66457
SDQ [nm]	0.442367	0.47824	0.442939	0.408333	0.369572	0.39462
SSC [1/µm]	0.17374	0.191549	0.178306	0.164417	0.158343	0.141028

Table S2. Sample ID, interplanar distance and carbon content.

Sample ID	Interplanar distance (nm)	Carbon content
Graphite	0.3458	-
GO	0.6019	0.068
TRGO-100	-	0.97
TRGO-200	-	2.26
TRGO-300	-	7.05
TRGO-400	0.3864	9.657
TRGO-500	0.3566	11.74

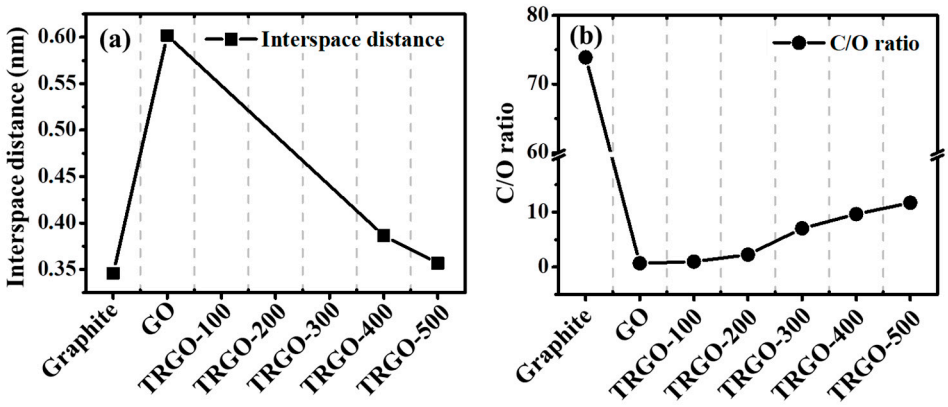

Figure S5. (a) Interspace distance and **(b)** C/O ratio as a function for graphite, GO and TRGO-100, TRGO-200, TRGO-300, TRGO-400 and TRGO-500.

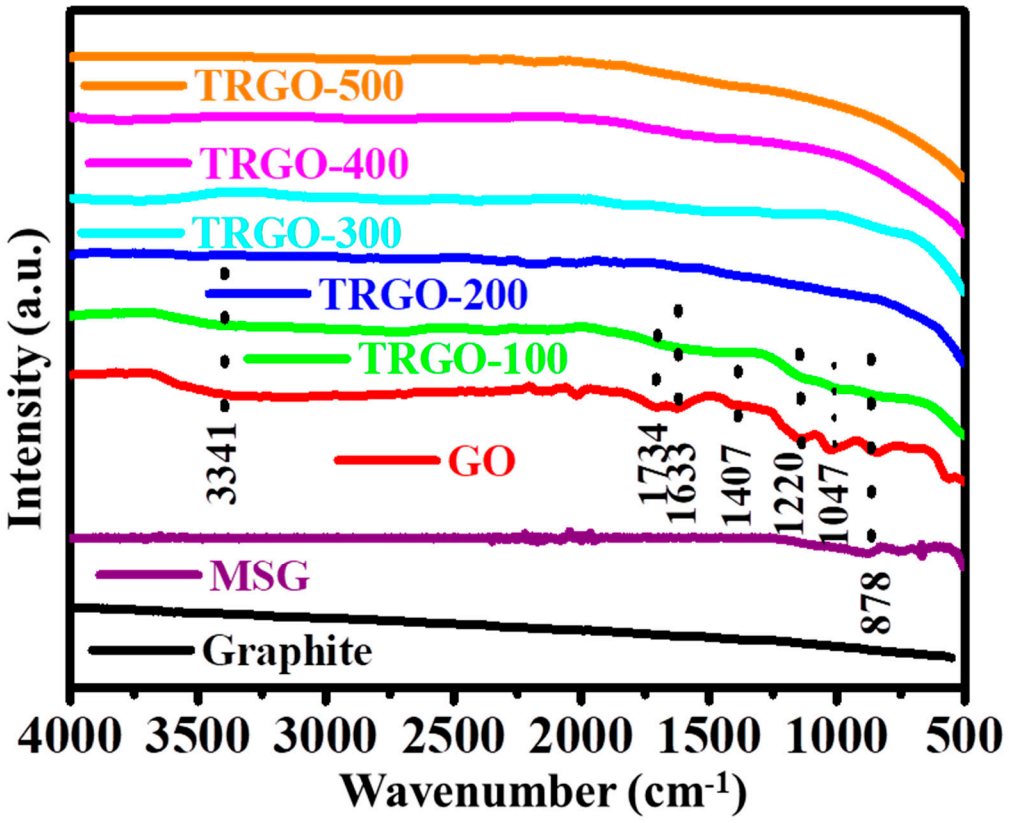

Figure S6. The FTIR of graphite, MSG, GO and TRGO samples.

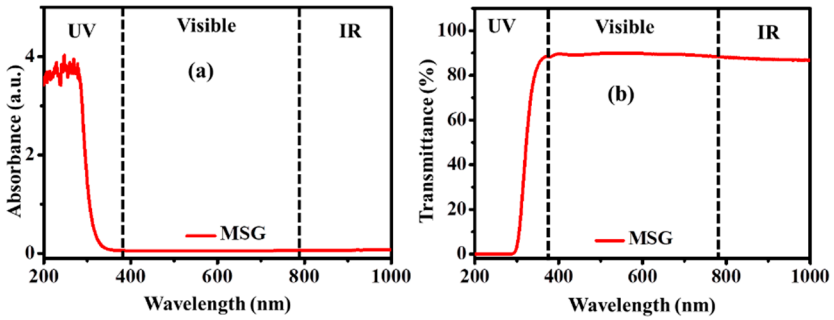

Figure S7. (a) Absorbance and **(b)** transmittance of microscope glass.

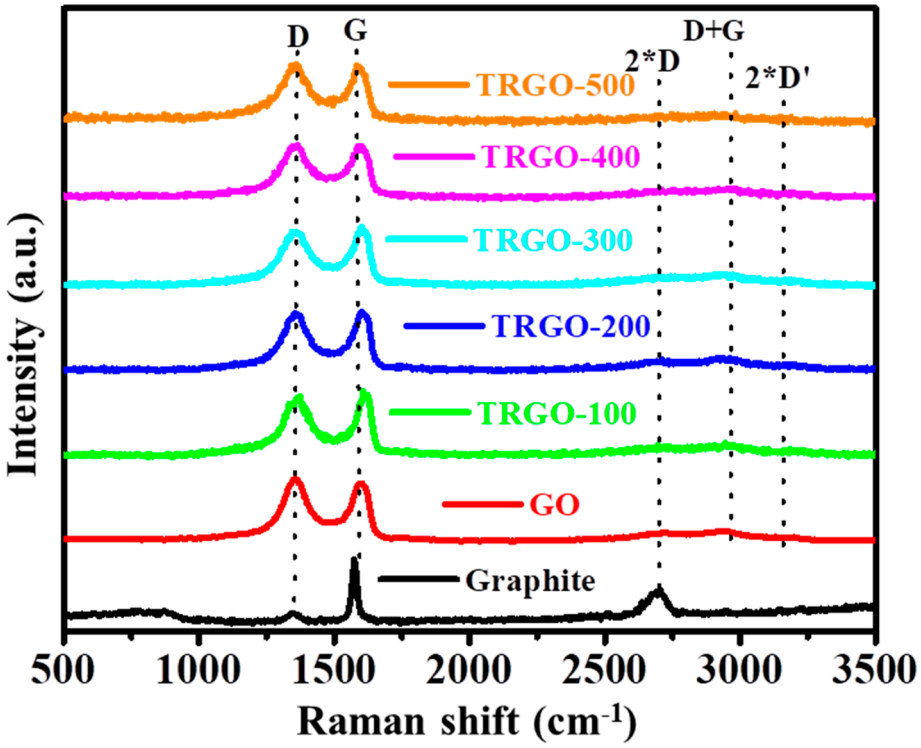

Figure S8. Raman spectra of graphite, GO and TRGO-100–TRGO-500.

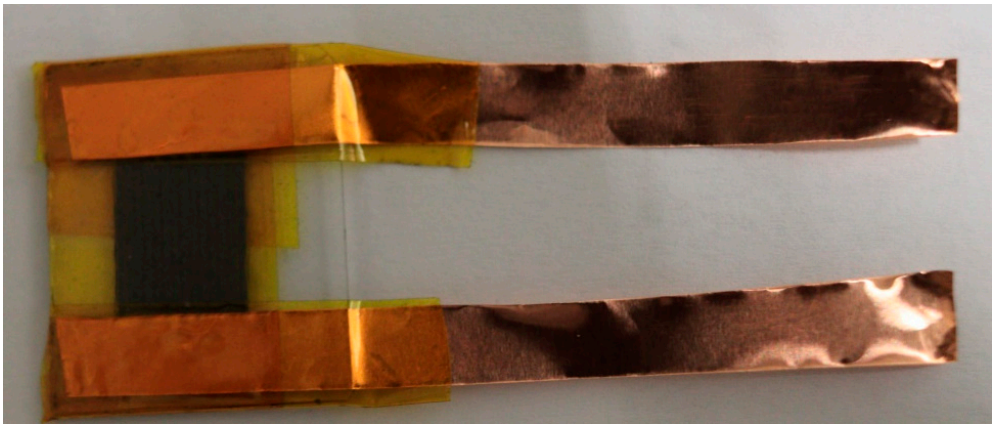

Figure S9. Digital image of μ-SC.

Table S3. Dimensions and parameters of μ-SC.

Parameters	μ-SC
Number of digits per unit area, n (cm^{-2})	14
Width, W (mm)	0.71
Length, L and Breadth, B (mm)	10
Interspace, i(μm)	38
Edge, E (mm)	4
Total surface area (mm^2)	100

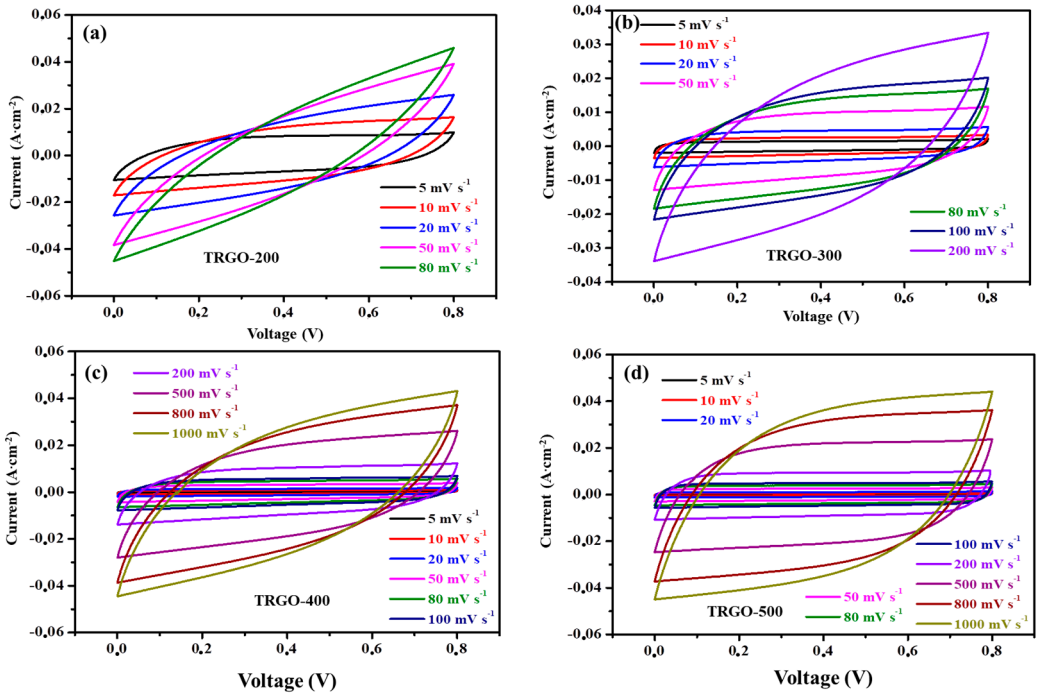

Figure S10 (a)–(d) CV curves of TRGO-200–TRGO-500.

The areal capacitance (C_{Areal}) displayed in Figure 8c and Table S4 of the TRGO samples was estimated from the CV curves using Equation (S1) [1–3]

$$C_{\text{Areal}} = \frac{\int_{V_i}^{V_f} i\,dV}{2\upsilon(V_f - V_i)A} \quad \text{(S1)}$$

where V_f and V_i are the final and initial values of the working potential (v), respectively. i, υ, and A are the current (mA), various scan rate (mVs^{-1}), and total surface area (cm^2) of the μ-SC including the interdigit space.

Table S4. The areal capacitance determined from the CV curve.

Scan rate mV s^{-1}	Areal capacitance (mF cm^{-2})			
	TRGO-200	TRGO-300	TRGO-400	TRGO-500
5	0.7074	0.1451	0.0444	0.0319
10	0.5421	0.1227	0.0382	0.0298
20	0.3773	0.1061	0.0348	0.0274
50	0.2085	0.0865	0.0301	0.0256
80	0.1498	0.0756	0.0282	0.0244
100	-	0.0695	0.0267	0.0239
200	-	0.0506	0.0234	0.0220
500	-	-	0.0179	0.0194
800	-	-	0.0148	0.0172

1000	-	-	0.0140	0.0159
1800				0.0149

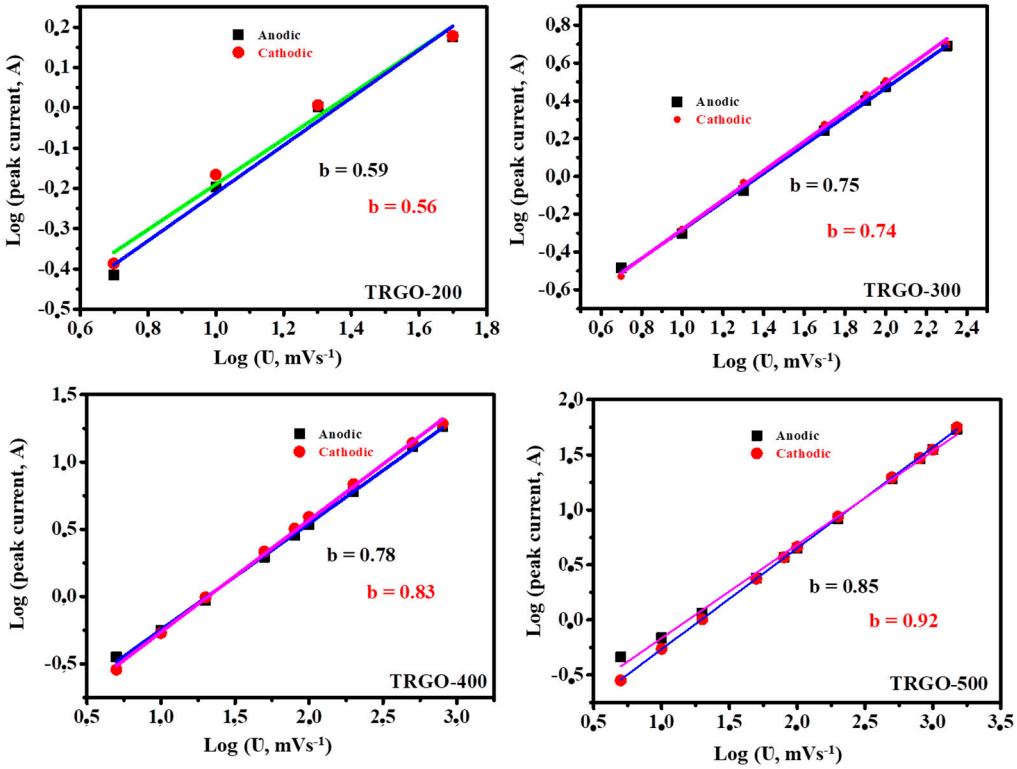

Figure S11. log I versus log υ curves for the anodic and cathodic currents at **(a)** TRGO-200, **(b)** TRGO-300, **(c)** TRGO-400 and **(d)** TRGO-500 reducing temperatures, respectively.

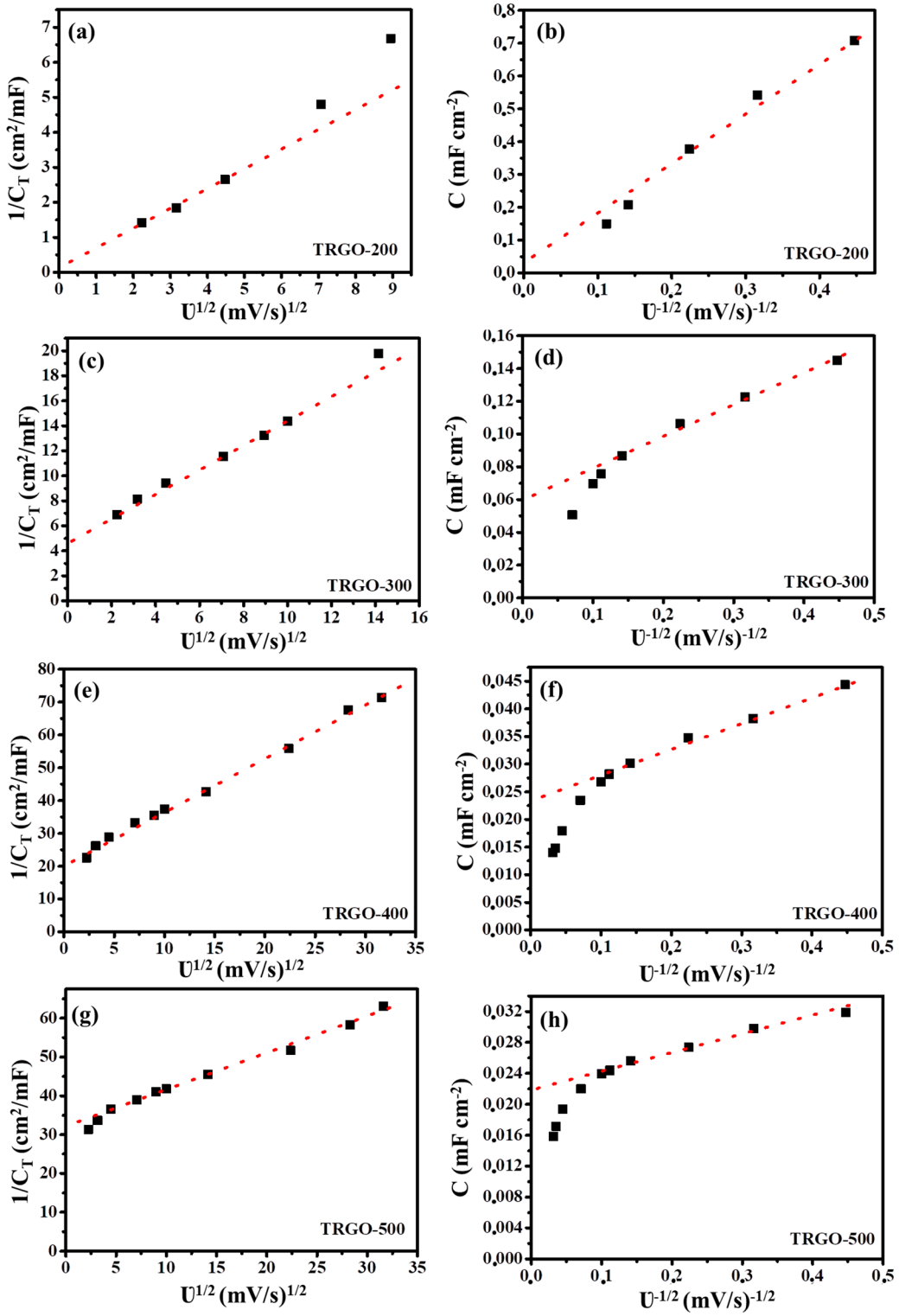

Figure S12 Trasatti's method for the TRGO micro-supercapacitors: **(a,c,e,g)** inverse capacitance as a function of square root of scan rate and **(b,d,f,h)** capacitance as a function of inverse square root of scan rate.

The Equation (S2) was used to calculate the diffusion (C_{pseudo}) contribution.

$$C_{\text{T}} = C_{\text{EDL}} + C_{\text{pseudo}} \quad \text{(S2)}$$

Table S5. Sample ID, maximum total capacitance, maximum EDL capacitance and maximum pseudocapacitance.

Sample ID	C_T (F g^{-1})	C_{EDL} (F g^{-1})	C_{pseudo} (F g^{-1})
TRGO-200	5.6524	0.0334	5.6190
TRGO-300	0.2058	0.0613	0.1445
TRGO-400	0.0497	0.0236	0.0261
TRGO-500	0.0311	0.0222	0.0089

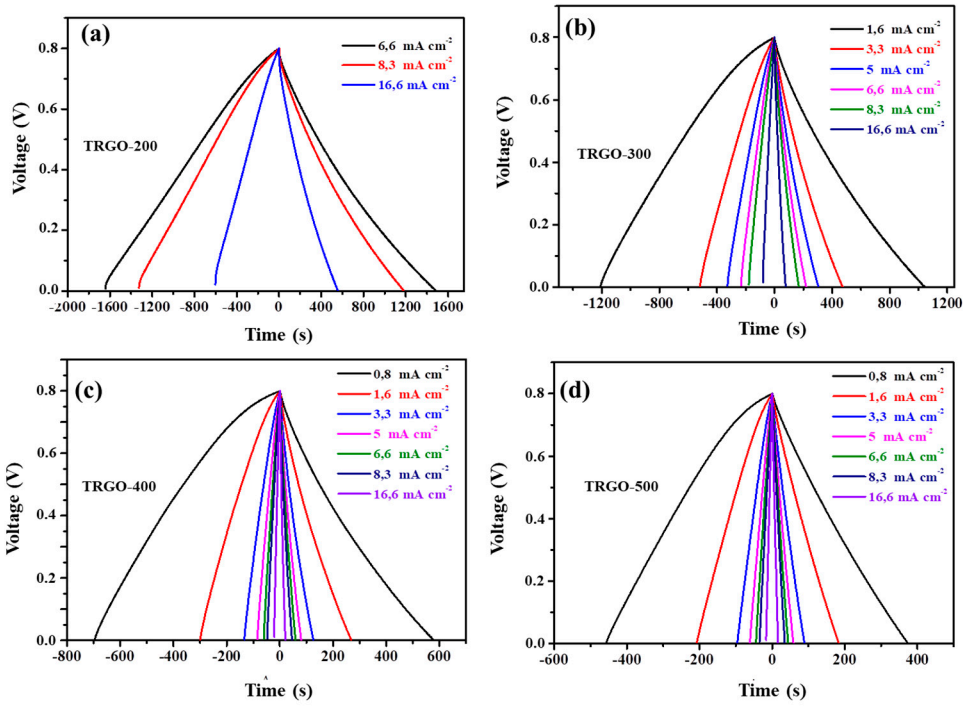

Figure S13. (a)–(d) GCD curves of TRGO-200–TRGO-500.

Table S6. The areal capacitance determined from the GCD curve.

Current density	Areal capacitance (mF cm^{-2})			
(μA cm^{-2})	TRGO-200	TRGO-300	TRGO-400	TRGO-500
0.083	-	-	0.0600	0.0387
0.16	-	0.2143	0.0536	0.0366
0.33	-	0.1952	0.0517	0.0367
0.5	-	0.1904	0.0501	0.0364
0.66	1.2255	0.1809	0.0481	0.0356
0.83	1.2262	0.1754	0.0472	0.0354
1.66	1.1569	0.1506	0.0434	0.0338

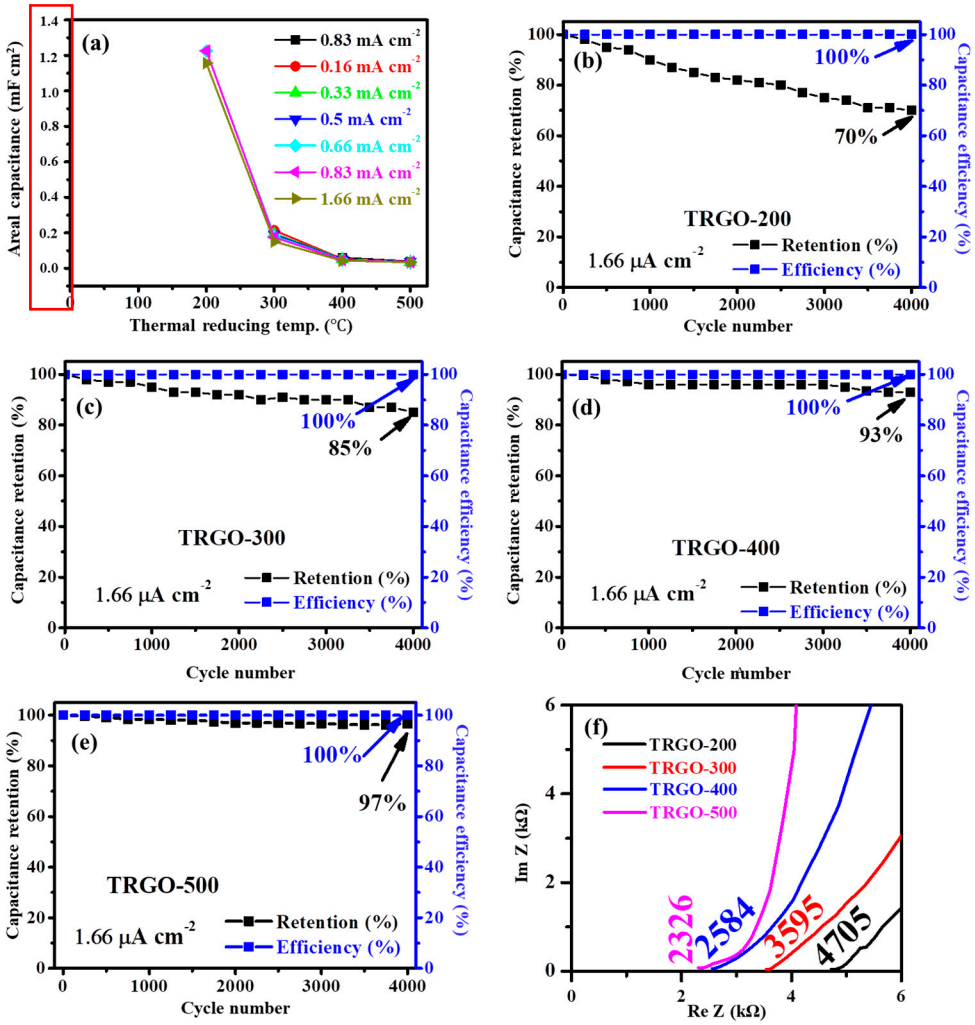

Figure S14. (a) Area capacitance as a function of reducing temperature at various current densities, **(b)–(e)** the capacitance retention and capacitance columbic efficiency of the TRGO sample and **(f)** EIS Nyquist plot at high frequency region.

The areal energy (E_{areal}) and power (P_{areal}) calculated from the below Equations (S3) and (S4)

$$E_{\text{areal}} = \frac{1}{3600\Gamma}\int iVdt \quad \text{(S3)}$$

$$P_{\text{areal}} = 3600 \times \frac{E_{areal}}{\Delta t} \quad \text{(S4)}$$

where Γ, $\int iVdt$ and Δt are the area or volume of the μ-SC, the integral of the discharge curve and discharge time, respectively.

Table S7. Sample ID, resistance electrolyte plus charge transfer resistance ($R_e + R_{ct}$), Warburg coefficient (σ_w) and ion diffusion coefficient (D).

Sample ID	Maximum specific power (W cm^{-2})	Maximum specific energy (W h cm^{-2})	$R_e + R_{ct}$ (Ω)	σ_w (Ω cm^2 s$^{-0.5}$)	D (cm^2 s^{-1})

TRGO-200	3.4006×10^{-5}	0.5024	4.71236	12.4831±0.002	4.3075×10^{-13}
TRGO-300	4.4506×10^{-5}	0.0183	3.52368	14.6329±0.001	3.1351×10^{-13}
TRGO-400	6.1950×10^{-5}	0.0044	2.53551	21.8812±0.001	1.4021×10^{-13}
TRGO-500	6.8788×10^{-5}	0.0028	2.26279	37.7070±0.002	4.7214×10^{-14}

The impedance ($Z(\omega)$) is expressed by Equation (S5)

$$Z(\omega) = \frac{1}{j\omega \times C(\omega)} \quad \text{(S5)}$$

Therefore,

$$Re\ C = \frac{Im\ Z(\omega)}{\omega|Z(\omega)|^2} \quad \text{(S6)}$$

$$Im\ C = \frac{Re\ Z(\omega)}{\omega|Z(\omega)|^2} \quad \text{(S7)}$$

where $Re\ Z(\omega)$ and $Im\ Z(\omega)$ are defined as

$$|Z(\omega)|^2 = Re\ Z(\omega)^2 + Im\ Z(\omega)^2 \quad \text{(S8)}$$

And

$$\omega = 2\pi f \quad \text{(S9)}$$

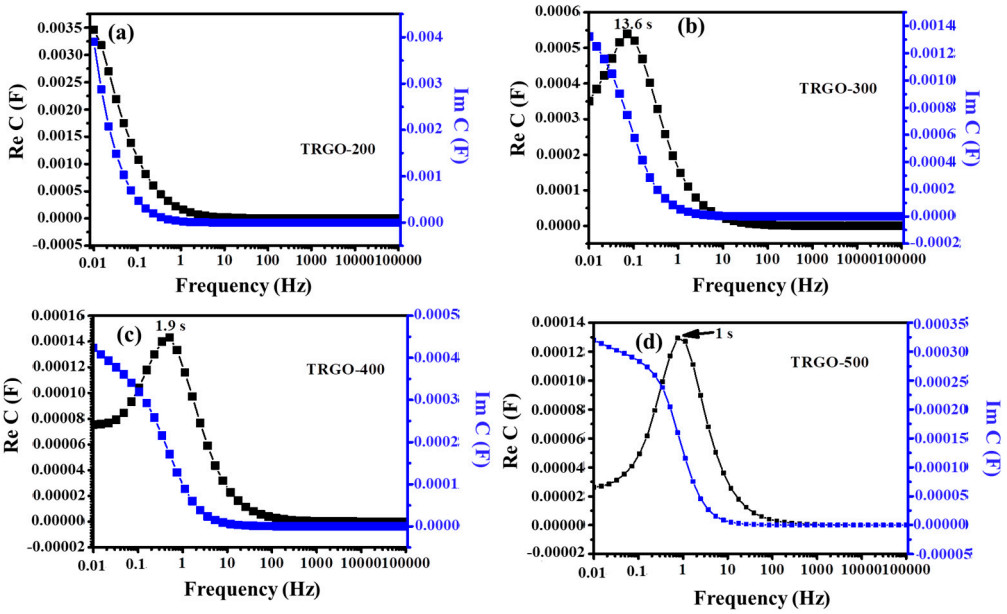

Figure S15. The frequency dependence of the Re C and Im C for **(a)–(b)** TRGO-200 to TRGO-500.

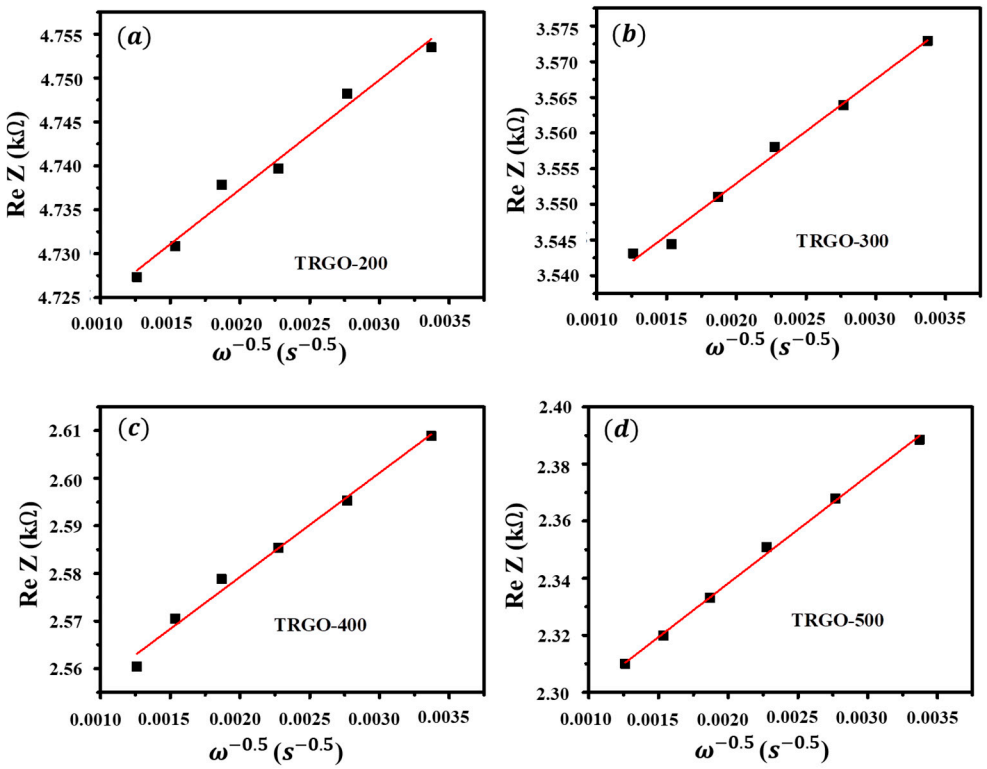

Figure S16. The relationship between Re Z and $\omega^{-0.5}$ at low frequencies for TRGO samples

Equation (S10) [4] was used to calculate ion diffusion coefficient (D)

$$D = 0.5\left(\frac{RT}{AF^2\sigma_w C}\right)^2 \quad \text{(S10)}$$

where R is the gas constant (8.314 J mol^{-1} K^{-1}), T is the temperature (298.5 K), A is the total area (cm^2) of the μ-SC fingers, F is the Faraday's constant (96,500C mol^{-1}) and C is the molar concentration of H^+ ions calculated using Equations (S11) and (S12).

The proton concentration $[H^+]$ of the used PVA/H_3PO_4 electrolyte was calculated using Equations (S11) and (S12).

$$Ph = -\log[H^+] \quad \text{(S11)}$$

$$[H^+] = 10^{-Ph} \quad \text{(S12)}$$

where, the Ph was measured to be 1.64 corresponding to $[H^+]$ of 0.023

Reference

1. Maphiri, V.M.; Rutavi, G.; Sylla, N.F.; Adewinbi, S.A.; Fasakin, O.; Man, N. Novel Thermally Reduced Graphene Oxide Microsupercapacitor Fabricated via Mask—Free AxiDraw Direct Writing. *Nanomaterials* **2021**, *11*, 1909.
2. Liu, L.; Ye, D.; Yu, Y.; Liu, L.; Wu, Y. Carbon-based flexible micro-supercapacitor fabrication via mask-free ambient micro-plasma-jet etching. *Carbon N. Y.* **2017**, *111*, 121–127. https://doi.org/10.1016/j.carbon.2016.09.037.
3. Li, J.; Levitt, A.; Kurra, N.; Juan, K.; Noriega, N.; Xiao, X.; Wang, X.; Wang, H.; Alshareef, H.N.; Gogotsi, Y. MXene-conducting polymer electrochromic microsupercapacitors. *Energy Storage Mater.* **2019**, *20*, 455–461. https://doi.org/10.1016/j.ensm.2019.04.028.
4. Cui, Y.; Zhao, X.; Guo, R. Improved electrochemical performance of La0.7Sr0.3MnO$_3$ and carbon co-coated LiFePO4 synthesized by freeze-drying process. *Electrochim. Acta* **2010**, *55*, 922–926. https://doi.org/10.1016/J.ELECTACTA.2009.08.020.